Circuit Model for Coupling Between MMIC's in Multichip Modules Including Resonance Effects

Robert W. Jackson, *Senior Member, IEEE,* and Zhaoyang Wang, *Student Member, IEEE*

***Abstract*— This paper describes a circuit model to be used for the approximate calculation of coupling between monolithic microwave integrated circuits (MMIC's) in a multichip module. The model is developed from basic electromagnetic principles and relies on the formation of equivalent electric dipoles to represent the complex currents on the various MMIC's within the module. The technique is suitable for use in layout-based circuit simulators and uses no numerical analysis.**

***Index Terms*— Coupling, electromagnetic coupling, MCA, MCM, multichip assembly, multichip module.**

I. Introduction

MICROWAVE modules generally consist of monolithic microwave integrated circuits (MMIC's) and supporting components enclosed in some type of housing or package [1], [2]. Fig. 1 illustrates such an assembly. It shows MMIC's embedded in an interconnecting substrate, which forms the upper layer of a multilayer substrate. A conducting cover is mounted on top and connects with vias to the ground planes below. This paper describes a computer-aided design (CAD) technique for use in predicting the parasitic coupling between the MMIC's in such modules.

Microwave CAD of a module currently consists of simulations where the MMIC's within are coupled using only circuit theoretic techniques. Electromagnetic coupling (relating to layout or packaging) is neglected. If, after building a module, it turns out that the neglected coupling significantly affects performance—e.g., causing oscillation—then the module package must often be redesigned. For low-cost packages, this is especially difficult and time consuming.

In principle, interchip coupling could be evaluated from a full electromagnetic simulation of the module and all the circuit currents in it. However, each MMIC may consist of a 100 or more components that emit energy to, and receive energy from, the other MMIC's in the module. Simulation of such a situation is currently unrealistic and the detail it would provide is not necessary. An approximate analysis which can be done quickly would be much more useful.

This paper describes in more detail the concept that was originally presented in [3]. The basic idea requires that MMIC's in a multichip assembly (MCA) be treated as collections of ideal electric dipoles in so far as determining the coupling field is concerned. This means that only averages of the currents on the MMIC surface must be determined. A similar principle is used for the fast multipole method for static and quasi-static computations of capacitance [4] or inductance. However, here we are dealing with complex fully dynamic circuits that are weakly coupled. In addition, the proposed technique is not a numerical analysis technique, but rather an approximate circuit modeling method that is intended for use in conjunction with circuit-simulation CAD, including active devices. It does not require any numerical electromagnetics and would not put the demands on memory and the central processing unit (CPU) that are normally associated with numerical electromagnetics. No numerical preprocessing or post processing of any significance is necessary.

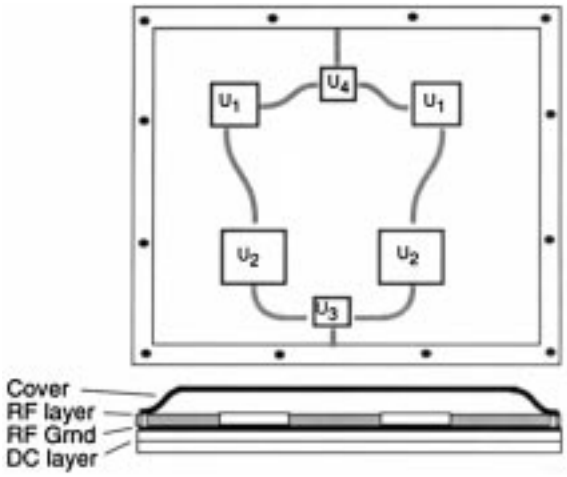

Fig. 1. Illustration of a multichip module.

In addition to detailing [3], this paper extends the range of the algorithm to include laterally enclosed packages. Section II describes the general algorithm. In Section III, the algorithm is applied to some test cases and the results compared to detailed full-wave simulation. The modification for laterally enclosed packages is presented in Section IV and verified by comparison to full-wave simulation in Section V.

II. The Algorithm

First, we overview the algorithm as illustrated in Fig. 2. The goal is to determine how much the performance of MMIC B is corrupted as a result of the fields generated by the currents on the components that comprise MMIC A. The figure shows an illustration of components in a hypothetical MMIC A, a

Manuscript received March 27, 1997; revised April 7, 1998. This work was supported by the Defense Advanced Research Projects Agency and by the Raytheon Company under a MAFET Thrust 1 contract.

The authors are with the Department of Electrical and Computer Engineering, University of Massachusetts Amherst, MA 01003 USA (e-mail: jackson@ecs.umass.edu).

Publisher Item Identifier S 0018-9480(98)04955-2.

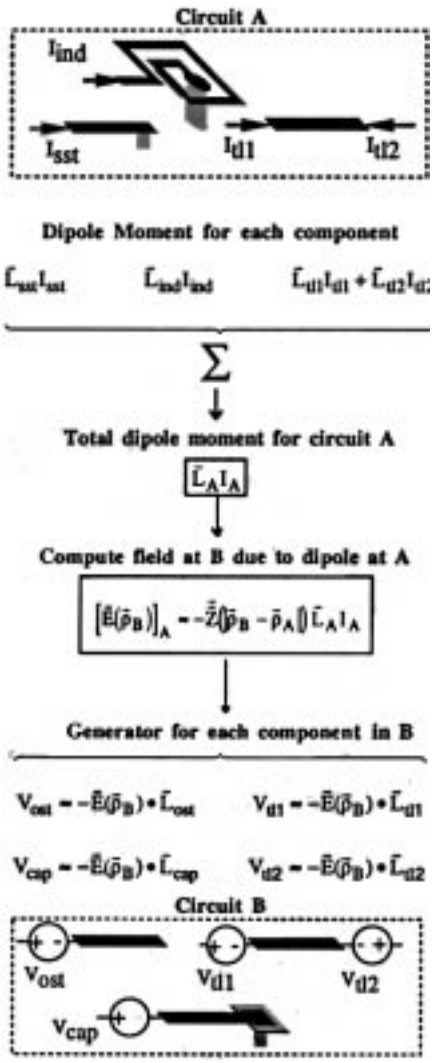

Fig. 2. Outline of algorithm for coupling MMIC A to MMIC B.

short-circuit stub, an inductor with one terminal grounded, and a length of transmission line. We define an *effective length* for each component, which determines how effectively it couples to the field inside the MCA. The effective length multiplied by the terminal current forms the *equivalent electric dipole* for that component. As far as field generation is concerned, MMIC A can be replaced by a cluster of equivalent electric dipoles. Since these dipoles are fairly closely space electrically, they can be combined to form an equivalent electric dipole for the entire chip. This macro-dipole is then used to calculate the approximate field at MMIC B or at other MMIC's in the MCA. On MMIC B, each component receives more or less energy depending on the component's effective length and orientation. The energy received induces voltages at the component terminal ports, which are modeled by voltage sources in series with each port terminal. A circuit simulator is then used to calculate the overall effect on MMIC B's performance.

The following approximations are used in determining the algorithm.

1) The separation between circuits A and B is large enough that they only couple to each other via the TM_0 parallel-plate wave. This implies that the conducting cover and ground plane are close enough to each other that all other parallel-plate waves are evanescent. This should be true for a majority of covered package structures [5].
2) The coupling between the MMIC's is small enough that their zeroth-order current distribution is not significantly changed from what it would be if no coupling existed. This is the same assumption that is made when the impedance of an antenna is calculated when another antenna is present some large distance away. If strong coupling were present, the general shape of currents A would be significantly changed by the presence of B. In our case, a package which allowed such strong coupling would be unusable and the accuracy of the coupling would not be an issue.
3) The dimensions of each MMIC are small relative to a TM_0 parallel-plate wavelength. Thus, the detailed current structure on the MMIC is not needed for the TM_0 field computation and only a small set of equivalent electric dipoles is necessary. This is a significant approximation and allows CPU and memory demands to be compatible with circuit simulation rather than full electromagnetic simulation. The assumption of small electrical size should remain valid up into the millimeter-wave range since the size of most MMIC's is on the order of a couple of millimeters and the TM_0 parallel-plate mode has a wavelength of the same order as a free-space wavelength. At still higher frequencies, or for more accuracy, a MMIC can be partitioned such that each subsection is represented by its own set of equivalent dipoles.

The details of the equivalent dipole algorithm are now described.

A. Approximate Field Evaluation

For the circuit model that we derive, we need the three components (x, y, z) of the electric field at B due to three components of current at A. For simplicity, we take only the x-directed fields due to x-directed currents as an example, and then list results for the remaining components in Appendix A. The rigorous evaluation of the fields is normally accomplished using a Green's function relation such as

$$E_x(x, y) = \iint dx'dy' G_{xx}(x, x', y, y') J_x(x', y') \qquad (1)$$

where G_{xx} is expressed as a spectral integral [5] and applies to a layered region of infinite extent. If currents A are sufficiently far from the field evaluation point on circuit B, then those field are primarily communicated by the TM_0 parallel-plate mode [5] (see Assumption 1). Equation (1) can then be simplified to

$$E_x(x, y) \approx \frac{-j}{2\beta^{\mathrm{TM}}} \mathrm{Res}[Q_{\mathrm{TM}}(\beta^{\mathrm{TM}})] \frac{\partial^2}{\partial x^2} R^{x\mathrm{TM}}(x, y) \quad (2a)$$

where

$$R^{x\mathrm{TM}}(x, y) \equiv \int_{-\infty}^{\infty}\int dx'dy' J_x(x', y') H_o^{(2)}(\beta^{\mathrm{TM}}|\vec{\rho} - \vec{\rho}'|) \qquad (2b)$$

and β^{TM} is the propagation constant of the TM_0 parallel-plate mode, is the solution of a transcendental equation, and can be determined by a standard root-finding algorithm. It only needs to be determined once per frequency for a given layered package and it may be complex if loss is present in any of the layers. Q_{TM} is an analytical function of β (see Appendix B), which contains information about the dielectric layers in the region around the MMIC. It has a pole at $\beta = \beta^{\mathrm{TM}}$ with an associated residue, $\mathrm{Res}[Q_{\mathrm{TM}}]$.

For simplicity, we limit the following derivation to x-directed currents and fields. The results for the y- and z-directions are listed in Appendix A. Assuming that x-directed currents on MMIC A are clustered around a location that we designate as $\vec{\rho}_{Ax}$, the Hankel function in (2b) can be expanded for $\vec{\rho}'$ near $\vec{\rho} = \vec{\rho}_{Ax}$. For MMIC currents of small extent relative to the TM-mode wavelength (Assumption 3), only the lowest order terms in the expansion are necessary. Equation (2b) then simplifies to

$$R^{x\mathrm{TM}}(x, y) \approx H_0^{(2)}(\beta^{\mathrm{TM}}|\vec{\rho} - \vec{\rho}_{Ax}|) \iint_{S_A} ds' J_x(\vec{\rho}') + \left[\vec{\nabla}' H_0^{(2)}(\beta^{\mathrm{TM}}|\vec{\rho} - \vec{\rho}'|)\right]_{\vec{\rho}'=\vec{\rho}_{Ax}} \cdot \iint_{S_A} ds'(\vec{\rho}' - \vec{\rho}_{Ax}) J_x(\vec{\rho}') \tag{3}$$

where S_A is the surface of MMIC A. The integral in the first term is the x-component of the electric dipole moment of the total current on MMIC A. The integral in the second term is the first moment of the current on MMIC A. In this paper, we neglect the second term. (It could, however, be used to improve the algorithm's accuracy.)

Equation (2) can, therefore, be approximated by

$$[\vec{E}_x(\vec{\rho}_B)]_A \approx -Z_{xx}(|\vec{\rho}_B - \vec{\rho}_{Ax}|) \iint_{S_A} ds' J_x(\vec{\rho}') \tag{4a}$$

where

$$Z_{xx}(|\vec{\rho} - \vec{\rho}_{Ax}|) = \frac{j}{2\beta^{\mathrm{TM}}} \mathrm{Res}[Q_{\mathrm{TM}}(\beta^{\mathrm{TM}})] \frac{\partial^2}{\partial x^2} H_0^{(2)}(\beta^{\mathrm{TM}}|\vec{\rho} - \vec{\rho}_{Ax}|). \tag{4b}$$

Note that only the integral of the current on A is needed to evaluate the field at B. The detailed current structure is not necessary. We will show that a circuit simulation can be used to determine this integral to a sufficient degree of accuracy. Also, the term Z_{xx} only has to be evaluated a few times, and it is easily evaluated. The Hankel function in (4b) can be approximated by its large argument forms. The y- and z-components of Z_{ij} are included in Appendix A.

B. Equivalent Dipoles and Effective Lengths

In what follows, we describe how to calculate in (4a) the integral of J_x and the equivalent source point $\vec{\rho}_{Ax}$. Basically, the integral of J_x is the equivalent dipole moment of the overall MMIC current and is approximately equal to the sum of dipole moments corresponding to each component within the MMIC. We designate the electric dipole moment of the overall MMIC A current by

$$L_{xA} I_A \equiv \iint_{S_A} ds J_x(x, y) \tag{5a}$$

where I_A is the terminal current of a presumed one-port MMIC and L_{xA} is the effective length of the sum of the x-directed currents in MMIC A. For an N-port MMIC, the integral would be replaced by a sum of dipoles

$$\iint_{S_A} ds J_x(x, y) = \sum_{n=1}^{N} I_A^{(n)} L_{xA}^{(n)} \tag{5b}$$

where $I_A^{(n)}$ is the terminal current at the nth port. Therefore, each port has a dipole associated with it defined by

$$I_A^{(n)} L_{xA}^{(n)} \equiv \left[\iint_{S_A} ds J_x(x, y)\right]_{I_A^{(i)}=0,\, i\neq n} \tag{5c}$$

where the nth x-directed dipole is determined by the x-directed current distribution when all but the nth port is open circuited.

The overall MMIC equivalent dipole in (5a) can be determined by summing the dipoles of the components within the MMIC. To form the component dipoles, we define an effective length for each component

$$\vec{L}_i = \frac{1}{I_i} \iint_{S_{Ai}} \vec{J}(x, y)\, dx\, dy \tag{6}$$

where S_{Ai} is the surface area associated with the ith component in MMIC A and I_i is the terminal current of the ith (presumed one-port) component. With this definition in mind, the dipole of the overall MMIC equation (5a) containing M components can be written as a the sum of the individual component dipoles

$$L_{xA} I_A = \sum_{i}^{M} \iint_{S_{Ai}} ds' J_x(\vec{\rho}') = \sum_{i}^{M} I_i L_{xi} \tag{7}$$

where the component terminal currents $\{I_i\}$ can be calculated by a standard circuit simulator. For a multiport MMIC, as described in (5c), various sets of $\{I_i\}$ will be generated depending on which port is excited and which ports are open circuited. Note that the number of ports in a MMIC will be very few and, thus, N in (5b) will be very small. On the other hand, there can be several hundred components in a MMIC, making M in (7) very large.

The effective component length (6) is a very fundamental part of this algorithm. Since it is normalized by the port current, it is a sort of form factor for the current on the component, and since the effective length depends on the integral of the current, knowing the detailed current characteristics is not necessary. An analytic expression for each $\vec{L}_i$ can be derived using a rough estimate of the current structure. It can then be stored along with a component's circuit model in a simulator's

library. For example, the effective length of an open-circuit stub of length ℓ oriented in the x-direction would be

$$\vec{L}_i = \frac{1}{I_i}\int_0^{\ell} I_i\Big(1-\frac{x}{\ell}\Big)\vec{u}_x\,dx = \frac{\ell}{2}\vec{u}_x. \tag{8}$$

At higher frequencies, a better approximation would result from using a sinusoidal current in the integrand. In such cases, the effective length will become slightly frequency dependent. At high frequencies, an effective length may have real and imaginary parts.

For a multiport component, each port has an effective length associated with it that can be determined from

$$\vec{L}_i^{(n)} = \left[\frac{1}{I_i^{(n)}}\iint_{S_{Ai}} \vec{J}(x,\,y)\,dx\,dy\right]_{I_i^{(n)}=0,\,i\neq n} \tag{9}$$

where $I_i^{(n)}$is the nth port of the ith component. The transmission-line section, shown in Fig. 2, is an example of such a case.

We now describe the evaluation of $\vec{\rho}_{Ax}$, the location vector for the x-directed MMIC equivalent dipole [see (4a)]. We have found that the most accurate results come from defining $\vec{\rho}_{Ax}$ by

$$\vec{\rho}_{Ax} \equiv \frac{\displaystyle\iint_{S_A} ds'\vec{\rho}'|J_x(\vec{\rho}')|}{\displaystyle\iint_{S_A} ds'|J_x(\vec{\rho}')|} = \left[\frac{\displaystyle\sum_i \vec{\rho}_{xi}|L_{xi}I_i|}{\displaystyle\sum_i |L_{xi}I_i|}\right] \tag{10}$$

where S_A refers to the area of MMIC A and $\vec{\rho}_{xi}$ locates the x-directed equivalent dipole for the ith component in MMIC A. $\vec{\rho}_{xi}$ is specified by

$$\vec{\rho}_{xi} \equiv \frac{\displaystyle\iint_{S_{Ai}} ds'\vec{\rho}'|J_x(\vec{\rho}')|}{\displaystyle\iint_{S_{Ai}} ds'|J_x(\vec{\rho}')|} \tag{11}$$

and S_{Ai} refers to the area associated with the ith component within MMIC A. For a multiport MMIC, the x-directed dipole associated with the nth port would be located at

$$\vec{\rho}_{Ax}{}^{(n)} \equiv \left[\frac{\displaystyle\iint_{S_A} ds'\vec{\rho}'|J_x(\vec{\rho}')|}{\displaystyle\iint_{S_A} ds'|J_x(\vec{\rho}')|}\right]_{I_A^{(i)}=0,\,i\neq n} \tag{12}$$

and can be evaluated in a manner similar to (10).

In general, each transmitting MMIC has a set of three (x, y, z) overall dipoles per port. The location of the x-directed dipole is different than the location of y-directed dipole and different also from the location of z-directed dipole. The dipole locations move around versus frequency since the distribution of current changes as a function of frequency.

C. Equivalent Voltage Generators

Lastly, we determine the voltages that are induced on the components in MMIC B. These voltages are then modeled in the circuit simulator using equivalent voltage sources connected in series with the terminals of each component. This is similar to the way that equivalent sources are used in noise analysis. For the ith one-port component in MMIC B, the port voltage can be found from the reciprocity relation [6]

$$V_i = -\frac{1}{I_i}\iint_{S_{Bi}} dxdy[\vec{E}(x,y)]_A\cdot\vec{J}_i(x,y) \tag{13}$$

where the subscript A indicates that the field in the integrand originates from circuit A. Assuming that $\vec{E}$ does not vary much over the extent of the ith component (Assumption 3), (13) can simplified to

$$V_i \approx -[\vec{E}(\vec{\rho}_B)]_A\cdot\frac{1}{I_i}\iint_{S_{Bi}} dxdy\vec{J}_i(x,y) = -[\vec{E}(\vec{\rho}_B)]_A\cdot\vec{L}_i \tag{14}$$

where $\vec{L}_i$ is the effective length of the ith component in MMIC B. If the ith component is a multiport, then the voltage at the nth port becomes

$$V_i^{(n)} \approx -[\vec{E}(\vec{\rho}_B)]_A\cdot\vec{L}_i{}^{(n)}. \tag{15}$$

The placement of the voltage generators is illustrated at the bottom of Fig. 2 for an open-circuit stub, a grounded capacitor–stub combination, and a transmission line.

To summarize, we refer again to Fig. 2. Each component in a MMIC has an effective length that can easily be precalculated and stored. The equivalent dipole for a component is determined by multiplying a component's effective length by the appropriate terminal current, as determined using standard-circuit CAD. The component dipoles are combined to create the overall dipole set that represents MMIC A. This set is then used in a simple approximate expression to find the fields at MMIC B. The dot product of the fields with the effective lengths of each of the MMIC B components yields the appropriate voltage generators. Circuit CAD can then be used to determine the resulting voltage at MMIC B's ports.

III. Comparison to Numerical Simulation: Anechoic Enclosure

In order to assess the accuracy of this algorithm, we compare its predictions to the those obtained from a full-wave analysis using Sonnet Software's *em* package.[1] The formulation described to this point assumes no sidewalls (infinite lateral extent). Since all *em* simulations take place in a fully enclosed computational box, we must make *em*'s box look infinitely large laterally by including a damping substrate layer just beneath the cover. The layer's loss is chosen to be large enough that a parallel-plate wave launched by the circuit is damped to a negligible level by the time it reflects from one of the simulator's sidewalls.

Fig. 3 shows the transadmittance between two one-port open-circuit stubs, each of which is fed at one end through

[1] *em* is a trademark of SONNET Inc., Liverpool, NY.

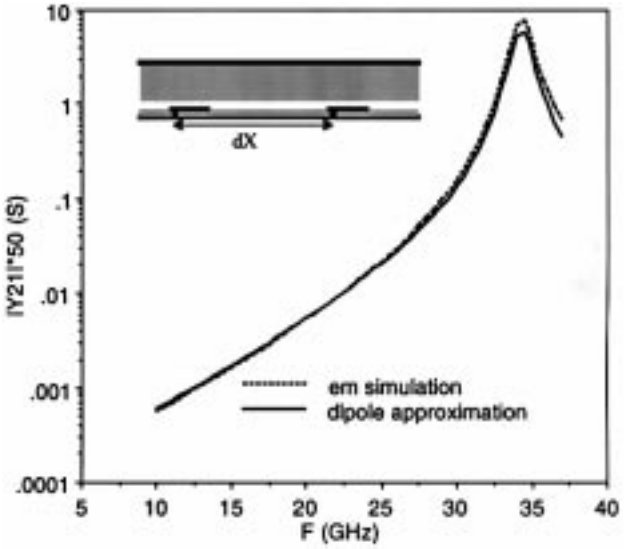

Fig. 3. Transadmittance between two one-port stubs. Side view in inset.

a via from the bottom plane of the test package. The stub dimensions are each 0.2 mm $\times$ 0.6 mm on the surface of a 0.1-mm substrate with $\varepsilon_r = 12.9$. A free-space layer (0.1 mm), a damping layer (0.7 mm, $\varepsilon_r = 12[1 - 10j]$), and a perfectly conducting cover make up the layers above the circuit. The stubs are colinear with centers separated by 3 mm.

The transmitting stub circuit is approximated by a z-directed dipole and an x-directed dipole. The effective length of the via is the substrate thickness 0.1 mm and the current through it is the port current I_1. Thus, the z-directed dipole has a moment $0.1I_1\hat{z}$ A-mm and is located at the via center. Using (8), we calculate the effective length of the stub to be 0.3 mm and, thus, the x-directed dipole moment is $0.3I_1\hat{x}$ A-mm. Using (11), we calculate the x-directed dipole's location to be 0.2 mm along the stub from via center. These two dipoles are used in conjunction with (4) and their counterparts in Appendix A to calculate the fields at stub B. The voltage source at the port of stub 2 is calculated from (15). It is $V_2 = -[0.3E_x + 0.1E_z]$ (we combined two sources for this simple circuit). Thus, what we have obtained at this point is the transimpedance between the stub ports. Because of the stub resonance, the transadmittance is a more interesting result. We obtained this by dividing the transimpedance by the square of the stub input impedance as obtained from *em* simulation of one stub. A circuit simulator with a good model of the stub/via is all that is necessary for this last step; *em* is not really required.

Fig. 3 compares the transadmittance determined from the dipole approximation to the transadmittance obtained entirely by em. Note that the curves are almost identical over a broad range of frequency and transadmittance.

Fig. 4 shows the S-parameter coupling between two two-ports for two different orientations Each two-port consists of a transmission line with a shunt connected open-circuit stub. The transmission line is a 1.4-mm length of microstrip fed at each end by vias to ports in the ground plane. All strip widths are 0.2 mm and all vias are 0.2-mm square. The stub length is 0.6 mm from transmission line edge to elbow and another 0.6 mm from elbow to stub end. The dielectric layers in the

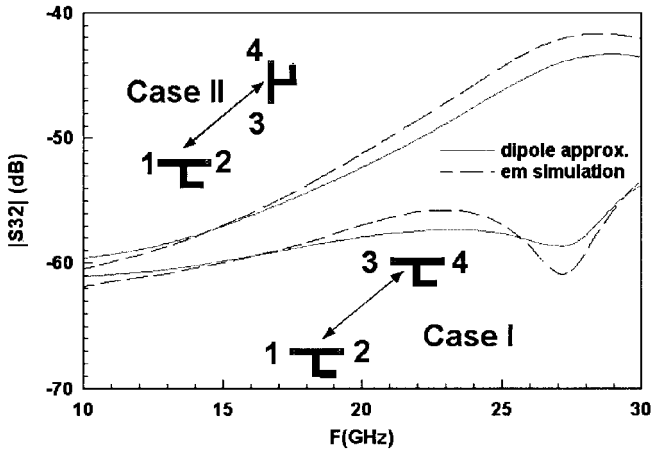

Fig. 4. Coupling between two two-port microstrip stub circuits separated by 5 mm. Case I with circuits co-oriented. Case II with one circuit rotated 90°.

structure are the same as the previous example. The centers of each circuit are separated from each other by 5 mm. In Case I, both circuits are oriented in the same way relative to one another. In Case II, the second circuit is rotated by 90°. Note this rotation has a very large effect on the coupling even though the distance between the two circuits has not increased.

Two sets (one for each port) of three dipoles (x, y, z) were used to compute the fields generated by a single circuit. The receiving circuit was subdivided such that nine voltage generators were used to model the coupling effect. Dividing this circuit into so many small pieces was not necessary. A division that required five generators would have produced similar results. Hewlett-Packard's Microwave Design System[2] was used to compute the effects of these sources at the input/output ports of the combined circuit.

The results show that the approximate method calculates the coupling within a few decibels of the more rigorous numerical calculation by *em*.

IV. Modified Algorithm for Finite-Size Enclosures

The algorithm as described above assumes an MCA which is of infinite lateral extent. Adding sidewalls to the package will cause package resonances to occur at high frequencies. Coupling is greatly enhanced at frequencies near a resonance. To reduce the effect, one can add a lossy damping layer, as was done for the preceding results, but it is difficult to determine how much damping is enough to completely eliminate resonance enhanced coupling and, therefore, we will usually need to include the influence of the walls in the algorithm. This will be accomplished using an image technique [5].

Each MMIC equivalent dipole creates a set of images in the sidewalls of the MCA. Our algorithm computes the field anywhere in an MCA of finite extent by converting the problem to an MCA of infinite extent populated by the primary dipole source and a set of image sources.

An x-directed dipole is taken as an example to show how the algorithm is modified for this situation. Fig. 5 shows the

[2]Microwave Design System is a trademark of Hewlett-Packard Company, Palo Alto, CA.

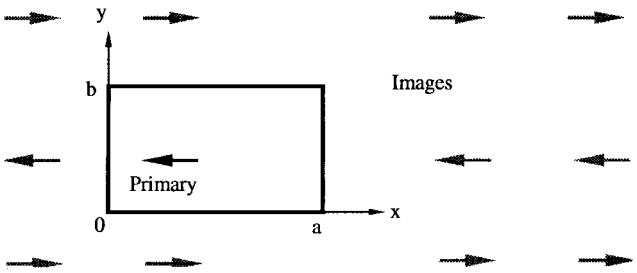

Fig. 5. Illustration of the MMIC equivalent dipole and its images.

primary and image dipoles. All the dipoles have strengths $L_{xA}I_A$. However, half of the image dipoles have the opposite direction to the primary one. Using (4), we can easily obtain the electric field at $\vec{\rho}_B$ radiated by $L_{xA}I_A$ and its images

$$\begin{aligned}[\vec{E}_x(\vec{\rho}_B)]_A &\approx -L_{xA}I_A \sum_{n=-\infty}^{\infty}\sum_{m=-\infty}^{\infty} \\ &\cdot \{Z_{xx}(|\vec{\rho}_B - \vec{\rho}_{AX} - (2na\hat{x}+2mb\hat{y})|) + Z_{xx} \\ &\cdot (|\vec{\rho}_B - (2a\hat{x} - \vec{\rho}_{AX}) - (2na\hat{x}+2mb\hat{y})|) - Z_{xx} \\ &\cdot (|\vec{\rho}_B - (2b\hat{y} - \vec{\rho}_{AX}) - (2na\hat{x}+2mb\hat{y})|) - Z_{xx} \\ &\cdot (|\vec{\rho}_B - (2a\hat{x}+2b\hat{y} - \vec{\rho}_{AX}) - (2na\hat{x}+2mb\hat{y})|)\}. \end{aligned} \tag{16}$$

We can do similar modifications on y- and z-directed dipoles $L_{yA}I_A$ and $L_{zA}I_A$. The number of image dipoles needed to evaluate the electric field at $\vec{\rho}_B$ depends on the loss in the damping layer and the required accuracy. For the example enclosure that we next describe, the accuracy is sufficient if all the image dipoles within a distance of ten times the box dimension are included in the summation.

V. Comparison to Numerical Simulation: Finite-Size Enclosure

Coupling between two test circuits in a moderate Q enclosure is computed using the full-wave analysis package em and using the modified circuit model algorithm described above. The loss tangent of the damping layer is 0.1. The box size is 8×8 mm. Otherwise, the layer structure and the two circuits in the box are the same as Case II described in Section III. Fig. 6 shows $|S_{32}|$ determined from a full-wave simulation and from our dipole approximation algorithm. Note the greatly increased coupling that occurs at the resonances introduced by the box. The result shows the good agreement between the two methods. In our algorithm, we include 675 image dipoles for every primary dipole. The total calculation time for the circuit model running in MDS is less than 1 min, which is at least two orders of magnitude faster than *em* run on an HP-715 workstation. For typically sized MMIC's, with 100 components within each MMIC, it would be impractical to run such a simulation using *em*.

VI. Conclusion

An algorithm has been described for computing the coupling between MMIC's in a multichip module. The

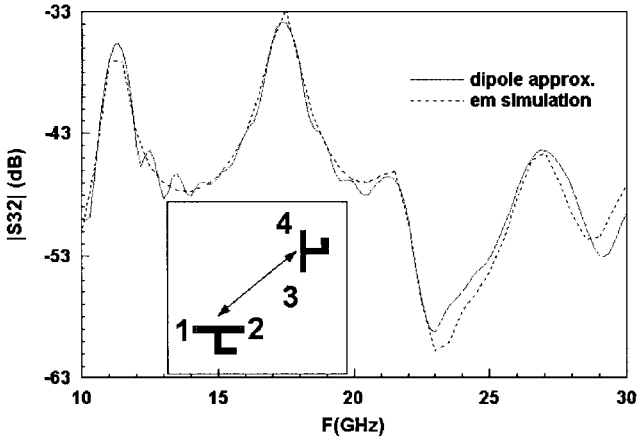

Fig. 6. Coupling between two two-ports in an box 8×8 mm in extent with a damping layer having a loss tangent of 0.1. The structure is otherwise identical to Case II in Fig. 4.

assumptions used in developing this algorithm are that: 1) the only coupling between MMIC's is based on the TM_0 parallel-plate mode; 2) the coupling between the MMIC's is weak enough that it does not significantly effect the current distribution on the transmitting MMIC; and 3) the size of the MMIC's involved is small relative to a TM_0 wavelength. This last assumption allows us to approximate the very complicated currents on the MMIC by a small set of dipoles and greatly simplifies the coupling calculation. We have verified the algorithm by comparing its predictions to a those of a numerically rigorous method of moments simulations.

The algorithm does not require any numerical electromagnetics other than finding the propagation constant of the parallel-plate TM_0 mode. Because it depends on averages of current—rather than the detailed current distribution—it does not require large memory resources. As a result, the algorithm can be used on arrays of MMIC's in a multichip module. Its organization is ideal for use in circuit/layout-based simulators.

This paper extends [3] by including more details of the technique and by introducing the modification that allows the use of the algorithm in enclosures with lateral sidewalls. Future work will address changes in coupling caused by coating a MMIC with a protective substance or by the presence of an inhomogeneous substrate.

Appendix A Coupling Matrix

The components of $\mathbf{Z}(|\vec{\rho} - \vec{\rho}_{A1}|)$ are

$$\begin{aligned} &Z_{xx}(|\vec{\rho} - \vec{\rho}_{A1}|) \\ &\quad \equiv \frac{j}{2\beta^{\mathrm{TM}}} \mathrm{Res}[Q_{\mathrm{TM}}(\beta^{\mathrm{TM}})] \frac{\partial^2}{\partial x^2} H_o^{(2)}(\beta^{\mathrm{TM}}|\vec{\rho} - \vec{\rho}_{A1}|) \end{aligned} \tag{A1}$$

$$\begin{aligned} &Z_{yy}(|\vec{\rho} - \vec{\rho}_{A1}|) \\ &\quad \equiv \frac{j}{2\beta^{\mathrm{TM}}} \mathrm{Res}[Q_{\mathrm{TM}}(\beta^{\mathrm{TM}})] \frac{\partial^2}{\partial y^2} H_o^{(2)}(\beta^{\mathrm{TM}}|\vec{\rho} - \vec{\rho}_{A1}|) \end{aligned} \tag{A2}$$

$$Z_{yx}(|\vec{\rho}-\vec{\rho}_{A1}|) \equiv \frac{j}{2\beta^{\mathrm{TM}}}\,\mathrm{Res}[Q_{\mathrm{TM}}(\beta^{\mathrm{TM}})]\frac{\partial^2}{\partial y\partial x}H_o^{(2)}(\beta^{\mathrm{TM}}|\vec{\rho}-\vec{\rho}_{A1}|) \tag{A3}$$

$$Z_{xy}(|\vec{\rho}-\vec{\rho}_{A1}|) \equiv Z_{yx}(|\vec{\rho}-\vec{\rho}_{A1}|) \tag{A4}$$

$$Z_{zx}(|\vec{\rho}-\vec{\rho}_{A1}|) \equiv \frac{-j\beta^{\mathrm{TM}}}{2k_{z1}^2\,d_1}\,\mathrm{Res}[Q_{\mathrm{TM}}(\beta^{\mathrm{TM}})]\frac{\partial}{\partial x}H_o^{(2)}(\beta^{\mathrm{TM}}|\vec{\rho}-\vec{\rho}_{A1}|) \tag{A5}$$

$$Z_{zy}(|\vec{\rho}-\vec{\rho}_{A1}|) \equiv \frac{-j\beta^{\mathrm{TM}}}{2k_{z1}^2\,d_1}\,\mathrm{Res}[Q_{\mathrm{TM}}(\beta^{\mathrm{TM}})]\frac{\partial}{\partial y}H_o^{(2)}(\beta^{\mathrm{TM}}|\vec{\rho}-\vec{\rho}_{A1}|) \tag{A6}$$

$$Z_{zz}(|\vec{\rho}-\vec{\rho}_{A1}|) \equiv \frac{-j(\beta^{\mathrm{TM}})^3}{2k_{z1}^4\,d_1^2}\,\mathrm{Res}[Q_{\mathrm{TM}}(\beta^{\mathrm{TM}})]H_o^{(2)}(\beta^{\mathrm{TM}}|\vec{\rho}-\vec{\rho}_{A1}|) \tag{A7}$$

$$Z_{xz}(|\vec{\rho}-\vec{\rho}_{A1}|) \equiv -Z_{zx}(|\vec{\rho}-\vec{\rho}_{A1}|) \tag{A8}$$

$$Z_{yz}(|\vec{\rho}-\vec{\rho}_{A1}|) \equiv -Z_{zy}(|\vec{\rho}-\vec{\rho}_{A1}|) \tag{A9}$$

$$k^2{}_{z1} = \varepsilon_1 k_0^2 - (\beta^{\mathrm{TM}})^2.$$

In (A1)–(A4), $Z_{ij} = -E_i/(L_jI_j)$ where i and j can be x or y. In (A5) and (A6),

$$Z_{zj} \equiv -\left[\int_0^{d_1} dz\, E_z\right] \Big/ L_jI_j \tag{A10}$$

where j can be x or y. Thus, in those cases, we are only considering the average E_z field in the (presumably) thin dielectric layer 1.

Appendix B
Q_{TM} Formula

The following notation describes Fourier-transform Green's function for the layered structure in Fig. 1. Note that $V = E$ or M

$$Q_{TV} = \frac{1}{Y_{LV}^{(1)} + Y_{RV}^{(2)}} = \frac{1}{Y_V} \tag{B1}$$

$$Y_{LV}^{(1)} = -jY_{TV}^{(1)}\cot(k_{z1}\,d_1)\,Y_{RV}^{(3)} = -jY_{TV}^{(3)}\cot(k_{z3}\,d_3) \tag{B2}$$

$$Y_{RV}^{(2)} = Y_{TV}^{(2)}\frac{Y_{RV}^{(3)} + jY_{TV}^{(2)}\tan(k_{z2}\,d_2)}{Y_{TV}^{(2)} + jY_{RV}^{(3)}\tan(k_{z2}\,d_2)} \tag{B3}$$

$$Y_{\mathrm{TM}}^{(i)} = \frac{e_{ri}k_o}{k_{zi}\eta_o}$$

$$Y_{\mathrm{TE}}^{(i)} = \frac{k_{zi}}{k_o\eta_o}$$

$$k_{zi}^2 = \varepsilon_{ri}k_0^2 - \beta^2, \qquad \mathrm{Im}(k_{zi}) < 0.$$

References

[1] G. Jerinic and M. Borkowski, "Microwave module packaging," in *IEEE Microwave Theory Tech. Symp. Dig.*, Albuquerque, NM, June 1992, pp. 1503–1506.

[2] A. K. Agrawal *et al.*, "Microwave module interconnection and packaging using multilayer thin film technology," in *IEEE Microwave Theory Tech. Symp. Dig.*, Albuquerque, NM, June 1992, pp. 1509–1511.

[3] R. W. Jackson and Z. Wang, "Circuit based model for coupling between MMIC's in multi-chip assemblies," in *IEEE Microwave Theory Tech. Symp. Dig.*, June 1997, Denver, CO.

[4] K. Nabors and J. White, "FastCap: A multipole accelerated 3-D capacitance extraction program," *IEEE Trans. Computer-Aided Design*, vol. 39, pp. 1447–1459, Nov. 1991.

[5] R. W. Jackson, "The use of sidewall images to compute package effects in MoM analysis of MMIC circuits," *IEEE Trans. Microwave Theory Tech.*, vol. 41, pp. 406–414, Mar. 1993.

[6] R. F. Harrington, *Time Harmonic Electromagnetic Fields.* New York: McGraw-Hill, 1961.

Robert W. Jackson (M'82–SM'88) received the B.S., M.S., and Ph.D. degrees from Northeastern University, Boston, MA, in 1975, 1979, and 1981, respectively.

From 1981 to 1982, he was an Assistant Professor in the Department of Electrical Engineering, Northeastern University. In 1982, he joined the University of Massachusetts, Amherst, where he is currently an Associate Professor. His primary research and teaching interests center on microwave and millimeter-wave electronics, especially integrated circuits. In particular, he has contributed in the areas of numerical modeling of microstrip and coplanar waveguide circuits, novel printed structures in coplanar waveguide, and the modeling of packages for microwave and millimeter-wave integrated circuits. He has also developed CAD routines for ferrite phase-shifter design and has consulted on topics connected with fiber optics for microwave applications.

Zhaoyang Wang (S'98) was born in Shanghai, China, in 1971. He received the B.S. degree in electrical engineering from the University of Science and Technology, China, in 1993, and is currently working toward the Ph.D. degree at the University of Massachusetts, Amherst.

From 1994 to 1996, he was a Research Assistant in the Laboratory for Millimeter Wave Devices and Space Applications, Department of Electrical and Computer Engineering, University of Massachusetts. His research included the investigation and characterization of solid-state detectors in the terahertz frequency range, focusing on superconducting hot electron bolometer (HEB) receivers. Since 1997, he has been working on circuit modeling of packaged MMIC's. His research interests also include MMIC design and RF CMOS circuit design.